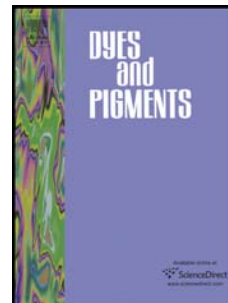


# Accepted Manuscript

Photophysicochemical behavior of carbazole derivatized zinc phthalocyanine in the presence of ZnO microparticles and when embedded in electrospun fibers

Phindile Khoza, Edith Antunes, Tebello Nyokong



PII: S0143-7208(13)00496-8

DOI: [10.1016/j.dyepig.2013.12.019](https://doi.org/10.1016/j.dyepig.2013.12.019)

Reference: DYPI 4216

To appear in: *Dyes and Pigments*

Received Date: 25 September 2013

Revised Date: 13 November 2013

Accepted Date: 18 December 2013

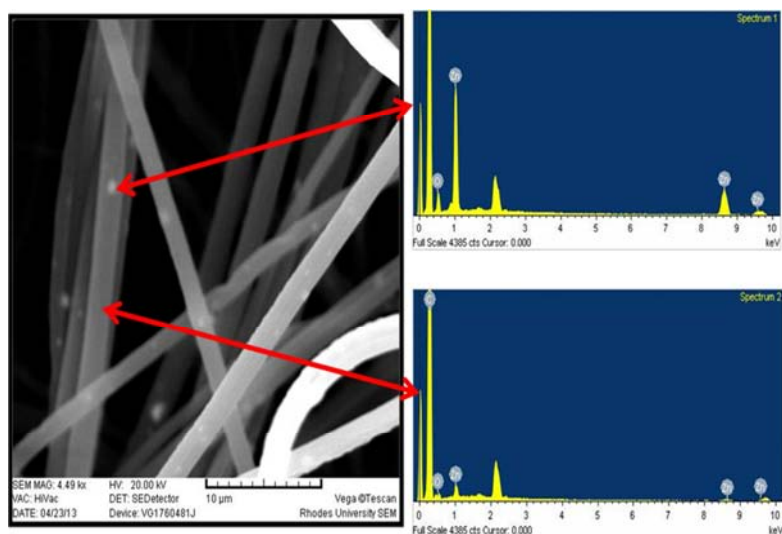
Please cite this article as: Khoza P, Antunes E, Nyokong T, Photophysicochemical behavior of carbazole derivatized zinc phthalocyanine in the presence of ZnO microparticles and when embedded in electrospun fibers, *Dyes and Pigments* (2014), doi: 10.1016/j.dyepig.2013.12.019.

This is a PDF file of an unedited manuscript that has been accepted for publication. As a service to our customers we are providing this early version of the manuscript. The manuscript will undergo copyediting, typesetting, and review of the resulting proof before it is published in its final form. Please note that during the production process errors may be discovered which could affect the content, and all legal disclaimers that apply to the journal pertain.

## Photophysicochemical behavior of carbazole derivatized zinc phthalocyanine in the presence of ZnO nanoparticles and when embedded in electrospun fibers

Phindile Khoza, Edith Antunes, Tebello Nyokong

zinc phthalocyanine complex tetrasubstituted with a carbazole functionality at the peripheral position (complex **4**) was conjugated to zinc oxide nanoparticles (ZnONPs) and electrospun into fibers. The singlet oxygen quantum yield values obtained were 0.25 and 0.20 for complex **4** and 4-ZnONPs, respectively.



**Photophysicochemical behavior of carbazole derivatized zinc phthalocyanine in the presence of ZnO microparticles and when embedded in electrospun fibers**

Phindile Khoza, Edith Antunes, Tebello Nyokong\*

*Department of Chemistry, Rhodes University, P.O. Box 94, Grahamstown, South Africa*

---

**Abstract**

The synthesis of a zinc phthalocyanine complex tetrasubstituted with carbazole functionality at the peripheral position (complex **4**) is reported. The singlet oxygen quantum yield of the complex was found to be 0.83 in dimethylformamide (DMF). The complex was subsequently conjugated to zinc oxide microparticles (ZnOMPs), the conjugation (formation of the amide bond) was confirmed by IR spectroscopy. The presence of ZnOMPs was found to reduce the singlet oxygen produced ( $\Phi_{\Delta}=0.63$ ) in DMF. Polystyrene electrospun fibers of complex **4** alone and its conjugate to ZnOMPs were found to be thermally stable. The singlet oxygen quantum yield of the modified electrospun fibers was determined in aqueous media with ADMA as a singlet oxygen quencher and were 0.25 and 0.20 for complex **4** and **4**-ZnOMPs embedded in fibers, respectively.

**Keywords:** zinc phthalocyanine, carbazole, polystyrene, ZnO microparticles, singlet oxygen quantum yield

\*Corresponding author. Tel.: +27-46-603 8260; fax: +27-46-622 5109. *E-mail address:* t.nyokong@ru.ac.za (T. Nyokong).

## 1. Introduction

Metallophthalocyanine (MPc) complexes are being extensively researched for their applications in for example electrocatalysis [1], nonlinear optics [2,3], chemical sensors [4,5] and photovoltaic cells [6]. The physical, chemical, electrochemical and other properties of these macrocycles are key to their suitability for the above applications, and can be obtained by careful selection of the central metal, type and position (peripheral and non-peripheral) of the substituents on the MPc ring [7-9]. MPc complexes are also well known as efficient photosensitizers in photodynamic therapy (PDT) of cancer [10-13]. Singlet oxygen is the cytotoxic species is involved in PDT.

On the other hand ZnO nanoparticles (ZnONPs) [14] and microparticles (ZnOMPs) [15] exhibit antimicrobial and anticancer activities through generation of reactive oxygen species (ROS), mostly hydroxyl radicals,  $H_2O_2$  and singlet oxygen [16,17]. Thus, linking the MPc with ZnOMPs (as is the aim of this work) will result in combined generation of ROS for improved antimicrobial and anticancer activities.

Zn phthalocyanine tetra substituted at the peripheral position with a carbazole moiety (Scheme 1, complex 4) is employed in this work, and its suitability as a photosensitizer examined. Carbazoles are also known to be good photosensitizers [18,19]. Thus the combination of the carbazole skeleton with the phthalocyanine ring is aimed at enhancing the photosensitizing activity of the Pc due to the synergistic effect. To further enhance the photosensitizing ability, complex 4 will conjugated to

ZnOMPs since both generate ROS. The conjugates of ZnOMPs with **4** will further be embedded in polystyrene (PS) electrospun fibers, for ease of recovery of the catalyst following future use in for example as antimicrobial agents. Electrospun fibers may be suitably functionalized for specific purposes. Our group has successfully incorporated phthalocyanines into a fiber mat for the photodegradation of organic pollutants in water [20]. The photophysicochemical behavior of complex **4** in the presence of ZnOMPs, in solution or when electrospun into fibers is investigated in this work. The conjugate of complex **4** with ZnOMPs is represented as **4**-ZnOMPs. The modified electrospun polystyrene (PS) fibers are represented as **4**/PS, ZnOMPs/PS and **4**-ZnOMPs/PS for **4** alone, ZnOMPs and **4**-ZnOMPs, respectively.

## 2. Experimental

### 2.1 Materials

Zinc acetate (99%), 1,8-diazabicyclo[5.4.0]undec-7-ene (DBU), 4-nitrophthalonitrile, 2-hydroxycarbazole, zinc phthalocyanine, *N,N*-dicyclohexylcarbodiimide (DCC), *N*-hydroxysuccinimide (NHS), anthracene-9,10-bis-methylmalonate (ADMA), citric acid and sodium hydroxide were purchased from Sigma Aldrich. Dimethylformamide (DMF), potassium carbonate, methanol, ethanol, 1-pentanol, acetone, diethyl ether and tetrahydrofuran (THF) were obtained from SAARCHEM.

### 2.2 Equipment

Ground state absorption spectra were recorded on a Shimadzu UV-2550 spectrophotometer. Fluorescence excitation and emission spectra were recorded on a Varian Eclipse spectrofluorimeter. Infrared spectra were recorded on a Perkin Elmer Spectrum 100 FT-IR spectrometer, while  $^1\text{H}$  NMR spectra were recorded on a Bruker AMX 600 NMR spectrometer.

Fluorescence lifetimes were measured using a time correlated single photon counting (TCSPC) setup (FluoTime 200, Picoquant GmbH). The excitation source was a diode laser (LDH-P-670 driven by PDL 800-B, 670 nm, 20 MHz repetition rate, 44 ps pulse width, Picoquant GmbH). Details have been provided before [21].

Mass spectral data were collected with a Bruker AutoFLEX III Smart beam TOF/TOF Mass spectrometer. The instrument was operated in positive ion mode using a  $m/z$  range of 500-3000 amu as described before [21]. X-ray powder diffraction (XRD) patterns were recorded on a Bruker D8 Discover XRD equipped with a Lynx Eye Detector, using  $\text{Cu K}_\alpha$  radiation ( $= 1.5405 \text{ \AA}$ , nickel filter). Details have been reported before [22].

Scanning electron microscope (SEM) images of the fiber alone or for 4/PS, ZnOMPs/PS and 4-ZnOMPs/PS were obtained using a JOEL JSM 840 scanning electron microscope. Transmission electron microscope (TEM) images were obtained using a Carl Zeiss Libra transmission electron microscope, at 100 kV accelerating voltage. Energy dispersive X-

ray spectroscopy (EDX) was acquired on a INCA PENTA FET coupled to the VAGA TESCA using 20 kV accelerating voltage. Fluorescence images of the fibers were taken with a DMLS fluorescence microscope; the excitation source was a high voltage mercury lamp.

Photo-irradiation for singlet oxygen quantum yield determinations for 4/PS, ZnOMPs/PS and 4-ZnOMPs/PS in water were carried out using a General Electric Quartz line lamp (300 W). A 600 nm glass cut off filter (Schott) and a water filter were used to filter off ultraviolet and infrared radiations respectively. An interference filter (Intor, 670 nm with a band width of 40 nm) was additionally placed in the light path before the sample. Light intensity was measured with a POWER MAX 5100 (Molelectron detector incorporated) power meter, and was found to be  $9.53 \times 10^{18}$  photons  $s^{-1}cm^{-2}$ . The thermal degradation properties of polystyrene and functionalized polystyrene electrospun fibers were studied using a thermogravimetric analyser (TGA) Shimadzu simultaneous differential thermogravimetric analysis thermal analyser (DTA-TG), at a heating rate of  $10 \text{ }^{\circ}C \text{ min}^{-1}$ , under nitrogen atmosphere, with a gas flow rate of  $120 \text{ mL min}^{-1}$ .

The phosphorescence of singlet oxygen at 1270 nm was used to determine the singlet oxygen quantum yield of complex 4 and 4-ZnOMPs in DMF. For these studies, an ultra-sensitive germanium detector (Edinburgh Instruments, EI-P) combined with a 1000 nm long pass filter (Omega, RD 1000 CP) and a 1270 nm band-pass filter (Omega, C1275,

BP50) were used. Experimental details have been provided before [23]. The singlet oxygen phosphorescence signal was compared with that of the ZnPc standard.

## 2.3. Photophysical and photochemical parameters

### 2.3.1. Fluorescence quantum yield

Fluorescence quantum yields ( $\Phi_f$ ) were determined by the comparative method (Eq. 1)

$$\Phi_f = \Phi_f^{std} \frac{F A^{std} n^2}{F^{std} A n_{std}^2} \quad (1)$$

where  $F$  and  $F^{std}$  are areas under the fluorescence emission curves of the sample and the standard, respectively.  $A$  and  $A^{std}$  are the absorbances of the analyte and the standard at the excitation wavelength, respectively;  $n$  and  $n^{std}$  are refractive indices of solvents used for samples and standard, respectively. ZnPc in DMF was used as a standard,  $\Phi_f = 0.30$  [24], for the determination of fluorescence quantum yields. The samples and the standard were both excited at the same relevant wavelength.

### 2.3.2. Singlet oxygen quantum yield ( $\Phi_\Delta$ )

The phosphorescence of single oxygen at 1270 nm was used to determine the singlet oxygen quantum yields of complex 4 and 4-ZnOMPs in DMF. Equation 2 was employed [25]:

$$I(t) = B \frac{\tau_D}{\tau_T - \tau_D} [e^{-t/\tau_T} - e^{-t/\tau_D}] \quad (2)$$

where,  $I(t)$  is the phosphorescence intensity of  $^1\text{O}_2$  at time  $t$ ,  $\tau_D$  is the lifetime of  $^1\text{O}_2$  phosphorescence decay,  $\tau_T$  is the triplet state lifetime of the standard or sample, and  $B$  is a coefficient involved in sensitizer concentration and  $^1\text{O}_2$  quantum yield.

The singlet oxygen quantum yields ( $\Phi_\Delta$ ) of complex **4** and **4**-ZnOMPs were determined using Equation 3:

$$\Phi_\Delta = \Phi_\Delta^{Std} \cdot \frac{B}{B^{Std}} \quad (3)$$

where  $\Phi_\Delta^{Std}$  is the singlet oxygen quantum yield of the standard ZnPc ( $\Phi_\Delta^{Std} = 0.56$  in DMF [26];  $B$  and  $B^{Std}$  are the coefficients of the sample and standard, respectively.

A chemical method was used to determine singlet oxygen quantum yield for **4**/PS and **4**-ZnOMPs/PS. The studies were carried out in an aqueous solution, using ADMA (concentration =  $5.8 \times 10^{-5}$  M). The decrease in the absorption for ADMA at 380 nm was monitored. The modified fiber (10 mg) was suspended in the solution containing ADMA and irradiated using the photolysis setup described above. The quantum yields ( $\Phi_{ADMA}$ ) were calculated using equation (4), using the molar extinction coefficient of ADMA in water,  $\log(\epsilon) = 4.1$  [27].

$$\Phi_{ADMA} = \frac{(C_o - C_t)V_t}{I_{abs}t} \quad (4)$$

where  $C_o$  and  $C_t$  are concentrations of ADMA before and after irradiation respectively;  $V_t$  is the volume of the solution irradiated and  $I_{abs}$  is defined by equation 5.

$$I_{abs} = \frac{\alpha A I}{N_A} \quad (5)$$

where  $\alpha = 1 - 10^{-A(\lambda)}$ ,  $A(\lambda)$  is the absorbance of the sensitizer at the irradiation wavelength,  $A$  is the irradiation area ( $2.5 \text{ cm}^2$ ),  $I$  is the intensity of light ( $9.53 \times 10^{18}$  photons  $\text{cm}^{-2} \text{ s}^{-1}$ ) and  $N_A$  is the Avogadro's constant. The absorbance used in equation 5 is that of complex 4 or 4-ZnOMPs on the fiber, determined by placing the fiber on a glass plate. The light intensity measured refers to the light reaching the spectrophotometer cell, and it is expected that some of the light may be scattered. Therefore,  $\Phi_{\Delta}$  values of complex 4 or 4-ZnOMPs on the fiber are estimates. The singlet oxygen quantum yields ( $\Phi_{\Delta}$ ) were calculated using equation 6 [28].

$$\frac{1}{\Phi_{ADMA}} = \frac{1}{\Phi_{\Delta}} + \frac{1}{\Phi_{\Delta}} \frac{k_d}{k_a} \frac{1}{[ADMA]} \quad (6)$$

where  $k_d$  is the decay constant of singlet oxygen and  $k_a$  is the rate constant of the reaction of ADMA with  $O_2$  ( $^1\Delta_g$ ). The intercept obtained from the plot of  $1/\Phi_{ADMA}$  versus  $1/[ADMA]$  gives the  $\Phi_{\Delta}$  values.

## 2.4. Synthesis

#### 2.4.1 4-(9H-carbazol-2-yloxy)-phthalonitrile (Scheme 1, complex 3)

A mixture of 2-hydroxycarbazole (**1**, 1.00 g, 6.6 mmol) and 4-nitrophthalonitrile (**2**, 1.1 g, 6.6 mmol) in DMSO (10 ml) was stirred under argon atmosphere at room temperature.  $K_2CO_3$  (10.07 g, 15 mmol) was added portion-wise to the reaction mixture and the mixture was stirred for 48 h. The reaction mixture was poured into ice water, and the precipitate was filtered off, washed with water and dried. The crude product was recrystallized from an ethanol: water mixture and air dried.

Yield: 1.46 g (70 %). FT-IR/ $cm^{-1}$ : 3078 (Ar-CH), 2961, 2834 (CH), 2230 (CN), 1579 (C C), 1475, 1456, 1442, 1383, 1325, (C-O-C), 1020, 1008, 962, 929, 792, 693.  $^1H$  NMR (DMSO-*d*6): 11.46 (1H, s, NH), 8.27 (1H,  $J= 8.4$  Hz, d, Ar-H), 8.19 (1H,  $J= 7.8$  Hz, d, Ar-H), 8.12 (1H,  $J= 8.8$  Hz, d, Ar-H), 7.82 (1H,  $J= 9.4, 2.5$  Hz, dd, Ar-H), 7.57 (1H,  $J= 8.1$  Hz, d, Ar-H), 7.50 (1H,  $J= 8.8$  Hz, dd, Ar-H), 7.43 (2H, m, Ar-H), 7.22 (1H,  $J= 7.4$ , t, Ar-H), 7.03 (1H,  $J= 8.4$  Hz, dd, Ar-H). Anal.  $C_{20}H_{11}N_3O$  : Calc: C, 77.66; H, 3.58; N, 13.58;. Found: C, 77.87; H, 4.21; N, 13.07.

#### 2.4.2. 2,(3)-Tetra(carbazol-2-yloxy)phthalocyaninatozinc(II) (Scheme 1, complex 4)

A mixture of zinc (II) acetate dihydrate (0.25 g, 1.1 mmol), **3** (1.36g, 4.4 mmol), DBU (3 drops) and 1-pentanol (10 mL) was stirred at 160 °C for 5 h under nitrogen atmosphere. After cooling, the solution was mixed with methanol. The green solid product was precipitated and collected by centrifuging at 5100 rpm for 10 min. The

crude product was washed with ethanol, acetone, n-hexane and diethyl ether. The green product was further purified by passing through silica gel using THF as the eluent.

Yield: 0.86 g (50 %). UV/vis (DMF):  $\lambda_{\max}$  nm (log  $\epsilon$ ); 680 (5.11), 612 (4.32), 362 (4.52).

FT-IR: ( $\nu_{\max}/\text{cm}^{-1}$ ): 3200 (NH), 3161 (Ar-H), 1576, 1077, 1110 (C-O-C), 1559 (C=N), 1412

$^1\text{H}$  NMR (DMSO- $d_6$ ):  $\delta$  ppm 11.46-11.25 (4H, b, NH), 9.46-9.32 (2H, b, Ar-H), 9.29-9.25 (1H, b, Ar-H), 9.00-8.92 (3H, b, Ar-H), 8.39-8.11 (10H, b, Ar-H), 7.95-7.69 (4H, b, Ar-H), 7.65-7.17 (24H, b, Ar-H). Anal.  $\text{C}_{80}\text{H}_{44}\text{N}_{12}\text{O}_4\text{Zn}$ : Calc. : C, 73.76; H, 3.40; N, 12.90; Found: C, 73.06; H, 3.79; N, 12.88. MALDI TOF-MS ( $m/z$ ): Calculated 1301; Found: 1302  $[\text{M}+\text{H}]^+$ .

#### 2.4.3. Synthesis of MPC-ZnOMPs conjugate

Citric acid capped ZnOMPs were synthesized as reported in literature [29,30], Scheme 2. Conjugation of the ZnO microparticles (ZnOMPs) with complex 4 was achieved as follows (Scheme 2). The carboxylic acid group of the citric acid capping of ZnO microparticles (0.014 g/mL in DMF), was activated with DCC (0.019 mg, 0.094 mmol) and NHS (3.62 mg, 0.031 mmol) for 16 h. Complex 4 (5 mg, 0.00384 mmol) dissolved in DMF (1 mL), was added dropwise into the mixture, and the reaction was allowed to continue for 24 h. The conjugate was purified by passing through a biobeads column using DMF as an eluent.

#### 2.4.4. Preparation of electrospun nanofibers

The electrospinning technique (with or without MPc complexes) has been described before [31,32]. Electrospun nanofibers were prepared as follows: A solution containing 2.5 g of polystyrene (PS), 3 mg of sample (complex 4, 4-ZnOMPs or ZnOMPs) and 10 mL DMF/THF(4:1) was stirred for 24 h to produce a homogeneous solution. The solution was then placed in a syringe fitted with a capillary needle. A potential difference of 20 kV was applied between the anode and cathode. The distance between the cathode (static fiber collection point) and anode (tip of capillary needle) was 15 cm. The pump rate was maintained at 0.05 mL/h.

### 3. Results and Discussion

#### 3.1. Synthesis and characterization of complex 4, ZnOMPs and 4-ZnOMPs

##### 3.1.1. Complex 4

Complex 4 was prepared by the cyclotetramerization of the phthalonitrile (**3**) in the presence of DBU and a metal salt. DBU acts as a nucleophilic base which allows for the reaction to proceed under mild conditions, while preventing the formation of side products (Scheme 1). A yield of 50% was obtained following repetitive purification by column chromatography. For the confirmation of the predicted structure, complex 4 was characterized by IR, MS and elemental analysis. After purification, the elemental analysis was in agreement with the proposed structure, confirming the purity of the prepared complex. MS revealed the presence of a molecular ion peak at 1302  $[M+H]^+$ , which further confirms the proposed structure. The higher Pc concentrations required

for  $^1\text{H}$  NMR, and the presence of isomers complicates phthalocyanine spectra. Nonetheless, the NMR spectrum of complex 4 showed aromatic peaks in the expected regions, with all protons accounted for, as reported in the experimental section.

### 3.1.2. ZnOMPs

The synthesis of ZnOMPs was achieved by using a well-established method reported by Shaheer *et al* [30]. The particles obtained were microflakes as reported in literature (Fig. 1a) [30]. The size of these microparticles ranged from 0.4 to 1.8  $\mu\text{m}$ , and their size distribution is shown in Fig 1b. The purity and crystallinity of the formed ZnOMPs were confirmed by the XRD, Fig. 2. The sharp, intense peaks in the XRD indicate that the ZnOMPs are highly crystalline. The peaks in the XRD powder pattern were observed at  $2\theta$   $31.95^\circ$ ,  $34.56^\circ$ ,  $36.40^\circ$ ,  $47.68^\circ$ ,  $56.83^\circ$ ,  $62.98^\circ$ ,  $66.53^\circ$ ,  $68.12^\circ$ ,  $69.27^\circ$  and  $76.97^\circ$  and were indexed to the (100), (002), (101), (102), (110), (103), (200), (112), (201), and (202) planes of the ZnO crystal respectively (as referenced by standard data file JSPC card number 01-075-0576). The formation of a pure hexagonal-wurtzite phase was confirmed by the XRD peaks at the (100), (002) and (101) planes for the ZnO structure. In addition, the narrow peaks imply a large particle size for the ZnOMPs, confirming the results obtained using SEM.

### 3.1.3. Complex 4-ZnNPs conjugate

Conjugation of complex **4** to ZnOMPs was achieved by activating the carboxylic acid functional group on the ZnOMPs with DCC which acts as a coupling agent (Scheme 2). The amide bond was formed via a condensation reaction between the activated carboxylic acid group on the ZnOMPs, and the secondary aromatic amine on the carbazole derivatized ZnPc (**4**). The formation of the amide bond was confirmed by the IR (Fig. 3), there is an appearance of a new peak at  $1750\text{ cm}^{-1}$ , due to the C=O stretching of the amide bond. The XRD pattern in Fig 2 shows the diffraction pattern of complex **4** and that of **4** conjugated to ZnOMPs. The XRD of the conjugate shows that the broad peak that is due to the Pc at  $2\theta = 20^\circ$  is very weak [33], the broadness is due to amorphous nature. The sharp peaks in the XRD pattern of the conjugate are due to ZnOMPs. Thus, the XRD pattern of the conjugate clearly shows the presence of highly crystalline ZnOMPs.

### 3.2. Ground state absorption spectra

One of the easiest ways of confirming the formation of metallophthalocyanines is through their UV-Vis spectra. Metallophthalocyanines exhibit two strong absorption regions, the B band ( $\sim 300\text{ nm}$ ), and the intense Q band in the NIR region. The UV-Vis spectra of complex **4** in different solvents are shown in Fig. 4A. The absorption spectrum of phthalocyanines is greatly influenced by the solvents basicity and the refractive index [34]. The red shifts in the Q band in Fig. 4A follows the refractive index of the solvents. Complex **4** was found to be soluble in most organic solvents, and showed monomeric behavior, as evidenced by a single narrow Q band. Upon

conjugating complex **4** to citric acid capped ZnOMPs, there was no significant shifting of the Q band of complex **4** (Fig. 4B).

The onset of the absorption for bulk ZnO at room temperature has been reported to be at 370 nm [35]. Citric acid capped ZnOMPs show a distinct absorption peak at ~ 340 nm (Fig. 5), the peak is blue shifted when compared to the bulk. The blue shift is due to the nanosize regime occupied by the particles, exhibiting the quantum confinement effect. The tailing of the absorption spectrum and the broadness of the emission peak is due to poor size dispersity of the microparticles.

### 3.3. Photophysical and photochemical studies

#### 3.3.1. Fluorescence studies

Fig. 6A shows the fluorescence emission, absorption and the excitation spectra of **4** in DMF. The excitation and absorption spectra are the same and are both mirror images of the emission spectra. The proximity (Table 1) of the Q band maxima of the absorption and excitation spectra suggest that the nuclear configuration of the ground state and excited state do not change upon excitation in all solvents. For the conjugate of complex **4** with ZnOMPs, the excitation band is split, most likely due to lowering of symmetry on excitation (Fig. 6B).

Fluorescence quantum yields ( $\Phi_F$ ) represent the fraction of the excited molecules that lose energy through fluorescence. The fluorescence quantum yields of the complexes are shown in Table 2. The  $\Phi_F$  value of **4** was found to be 0.12 (Table 2), the  $\Phi_F$

calculated is lower than that of the unsubstituted ZnPc ( $\Phi_F = 0.30$  [24]), implying that the substituent has an effect on the photophysical behavior of the ZnPc, as reported before [7]. The conjugate was found to give the same fluorescence quantum yield as complex 4.

Fluorescence lifetime ( $\tau_F$ ) refers to the time a molecule spends in its excited state before returning to the ground state. The fluorescence decay curve for 4 is shown in Fig. 7a. A mono exponential decay curve was obtained for the Pc, further confirming the purity of the prepared molecule. Due to the fluorescence quenching induced by the substituent, the low fluorescence quantum yield of 4 was accompanied with a short fluorescence lifetime when compared to the unsubstituted ZnPc in the same solvent. The conjugate of complex 4 with ZnOMPs gave a double exponential decay, with decrease in lifetime, Fig. 7b and Table 2. The presence or the evolution of two fluorescence lifetimes has been attributed to the different orientations of the phthalocyanines on the microparticles, with each orientation giving rise to a different fluorescence lifetime [36].

### 3.3.2. Singlet oxygen quantum yield studies

Singlet oxygen quantum yield ( $\Phi_\Delta$ ) is a measure of the efficiency of singlet oxygen generation for a given photosensitizer. Singlet oxygen is the chief cytotoxic species that is responsible for different applications. Singlet oxygen is formed via the interaction of the triplet state of the photosensitizer with the ground state molecular

oxygen. Factors which determine the magnitude of the singlet oxygen quantum yield include, the triplet state energy, ability of the substituent and the solvent to quench singlet oxygen, and the efficiency of the energy transfer between the triplet excited state and the ground state molecular oxygen. Complex 4 showed a high singlet oxygen quantum yield ( $\Phi_{\Delta} = 0.83$ ), proving its great potential for application as a photosensitizer. The high singlet quantum yield can be attributed to the capabilities of the carbazole ligand on its own to produce singlet oxygen. On conjugating complex 4 to ZnOMPs, there was a decrease in the amount of singlet oxygen produced ( $\Phi_{\Delta} = 0.64$ ). ZnOMPs have been reported to produce singlet oxygen. In this work, only the Q band of the Pc was excited. Therefore, the value of singlet oxygen obtained does not account for the singlet oxygen produced by ZnOMPs (which absorbs at higher energies than the complex 4). Nonetheless, the presence of ZnOMPs quenched the singlet oxygen produced by complex 4 alone.

### 3.4. Characterization of the electrospun fibers

#### 3.4.1. Scanning electron microscopy

Functionalized electrospun PS fibers (4/PS, ZnOMPs/PS and 4-ZnOMPs/PS) were characterized by the scanning electron microscopy. The electrospun fibers were cylindrical and un-branched with relatively smooth surfaces, Fig. 8. Electrospun polystyrene alone gave diameter sizes in a range of 3-4  $\mu\text{m}$  (Fig 8a). The diameters for 4/PS, ZnOMPs/PS and 4-ZnOMPs/PS ranged between 3 to 6  $\mu\text{m}$ . Functionalizing

fibers with ZnOMPs produced nanofibers which showed “white spots” embedded within (Fig. 8d). The spots were proven to be ZnO microparticles by EDX (Fig. 8e). The EDX (Fig. 8e) shows the elemental composition of these spots, and clearly outlines the high concentration of Zn and O as compared to neighboring areas (i.e. areas without white spots (Fig. 8f)). The idea behind electrospinning 4-ZnOMPs conjugate was to obtain an optimal nanocomposite for various applications including waste water disinfection. Nanofibers prepared are insoluble in water, making it easy to recover the fiber after use. The insolubility of complex 4 and the conjugate in water is also an advantage, as this implies that the content of the fiber will not leach out when used in aqueous media.

#### 3.4.2. Fluorescence microscopy

The ability of the nanofibers to emit light upon functionalization with complex 4 was examined with the fluorescence microscopy. ZnOMPs/PS (Fig. 9a) showed fluorescent spots, and the image correlates to that obtained from the SEM, further confirming that the fluorescent spots, or the whitish spots observed on the SEM are ZnOMPs embedded within the fiber. In the presence of complex 4, the fiber is observed to have remarkable emission upon excitation (Fig. 9b). Similar fluorescence was observed with excitation of the 4-ZnOMPs/PS (Fig.9c), albeit a weaker emission.

#### 3.4.3. TGA/DTA

The effect of heat on the prepared nanofibers was examined by thermal analysis. Changes in weight with increase in temperatures were monitored by thermogravimetric analysis (TGA). Fig. 10A shows that the modified fibers are slightly more stable than polystyrene alone. Differential thermogravimetric analysis (DTA) was acquired simultaneously with the thermogravimetric analysis; therefore, the results obtained are comparable. DTA gives the apparent degradation temperature and the derivative weight losses of the composites and polystyrene alone are shown in Fig.10B. The DTA curve of ZnOMPs/PS is clearly shifted to higher temperatures, indicating the greater thermal stability of the composite. The thermal stabilities of complex 4/PS and 4-ZnOMPs/PS were found to be similar, and slightly improved when compared to pristine polystyrene, as judged by the small shift to higher temperatures.

#### 3.4.4. UV-Vis spectra and XRD patterns

The fibers 4/PS, ZnOMPs/PS and 4-ZnOMPs/PS were not soluble in water but could be dissolved in toluene, with the aim of examining the integrity of the components of the modified fiber. UV-Vis spectra of the fiber composites (in toluene) are shown in Fig. 11, with a characteristic Q band at 683 nm. The integrity of the components (complex 4 or 4-ZnOMPs) in the electrospun fiber are not compromised upon electrospinning, since there were no changes in the Q band maxima. The XRD pattern of the electrospun fibers is shown in Fig. 12. The XRD pattern of PS shows a broad peak at  $2\theta = 20^\circ$ , where phthalocyanines also show a peak [33] as observed in Fig. 2. This broad

peak for PS is close to the 002 reflection peak for carbon [33]. The broadness of the peak is an indication of the amorphous nature of polystyrene electrospun fibers. Functionalization of polystyrene gave diffraction patterns that are mainly from polystyrene, there were no significant changes on the diffraction pattern of polystyrene upon functionalization (Fig 12).

#### 3.4.5. Singlet oxygen quantum yield determination

The singlet oxygen generation abilities of 4/PS and 4-ZnOMPs/PS were determined using the absolute method with ADMA as a quencher. Although the values obtained are an estimate of the singlet oxygen produced by complex 4, they are extremely useful for comparative purposes. Fig. 13 shows the degradation of ADMA in the presence of 4/PS. There is evidence of photo-conversion of ADMA due to the singlet oxygen produced by the phthalocyanine within the fiber. It is important to note that complex 4 did not leach out into solution during photolysis (there is no Q-band absorption). Singlet oxygen quantum yield values of 0.25 were obtained for 4/PS while 4-ZnOMPs/PS gave a singlet oxygen value of  $\Phi_{\Delta} = 0.20$ , Table 2. These values were found to be quite low, this is expected for experiments carried out in aqueous media since water is known to quench singlet oxygen [34]. Although the  $\Phi_{\Delta}$  values are estimates, they do give an indication as to how effective the fiber will be as an antimicrobial agent or a photocatalyst.

## Conclusions

Herein, we have reported on the synthesis and characterization of the carbazole derivatized zinc phthalocyanine (complex **4**). The complex showed remarkable photochemical behavior in DMF, with singlet oxygen quantum yield of 0.83. Upon conjugating the complex to ZnOMPs, the singlet oxygen quantum yield decreased (0.63). The composites showed greater thermal stability than polystyrene alone. The singlet oxygen quantum yields (in water) of the functionalized nanofibers were found to be 0.25 and 0.20 for **4**/PS and **4**-ZnOMPs/PS respectively.

#### **Acknowledgements**

This work was supported by the Department of Science and Technology (DST) Innovation and National Research Foundation (NRF), South Africa through DST/NRF South African Research Chairs Initiative for Professor of Medicinal Chemistry and Nanotechnology as well as Rhodes University and DST/Mintek Nanotechnology Innovation Centre (NIC) - Sensors, South Africa

**References:**

1. Baker RC, Wilkinson DP, Zhang JJ. Comparison of Two New Substituted Iron Phthalocyanines as Electrocatalysts for the Oxygen Reduction and Hydrazine Oxidation Reaction. *ECS Trans* 2009; 16: 43-61.
2. Britton J, Litwinski C, Durmus M, Chauke V, Nyokong T. Optical limiting behavior of ring substituted zinc, indium and gallium phthalocyanines in the presence of quantum dots. *J Porphyr Phthalocya* 2011; 15: 1239-1249.
3. Díaz-García MA, Nonlinear optical properties of phthalocyanines and related Compounds. *J Porphyr Phthalocya* 2009; 13: 652-667.
4. ZiyaÖztürk Z, Kılınç N, Atilla D, GülGürek A, Ahsen V. Recent studies chemical sensors based on phthalocyanines. *J Porphyr Phthalocya* 2009; 13: 1179-1187.
5. Muzikante I, Parra V, Dobulans R, Fonavs E, Latvels J, Bouvet M. A Novel Gas Sensor Transducer Based on Phthalocyanine Heterojunction Devices. *Sensors* 2007; 7: 2984-2996.
6. Walter MG, Rudine AB, Wamser CC. Porphyrins and phthalocyanines in solar photovoltaic cells. *J Porphyr Phthalocya* 2010; 14: 759-792.
7. Nyokong T. Effects of substituents on the photophysical and photophysical properties of main group metal phthalocyanines. *Coord Chem Rev* 2007; 251: 1707-1722.
8. Nemykin VN, Lukyanets EA. Synthesis of substituted phthalocyanines. *ARKIVOC* 2010; 1: 136-208.

9. Chidawanyika W, Nyokong T. Spectroscopic and photophysical behavior of novel cadmium phthalocyanines derivatives tetra substituted at the alpha and beta positions. *J Photochem Photobiol A-Chem* 2009; 202: 99-106.
10. Lukyanets EA. Phthalocyanines as Photosensitizers in the Photodynamic Therapy of Cancer. *J Porphyr Phthalocya* 1999; 3: 424– 432.
11. Whitacre CM, Feyes DK, Satoh T, Grossmann J, Mulvihill JW, Mukhtar H, Oleinick NL. Photodynamic Therapy with the Phthalocyanine Photosensitizer Pc 4 of SW480 Human Colon Cancer Xenografts in Athymic Mice. *Clin Cancer Res* 2000; 6: 2021-2027.
12. Kolarova H, Tomankova K, Bajgar R, Kolar P, Kubinek R. Photodynamic and Sonodynamic Treatment by Phthalocyanine on Cancer Cell Lines. *Ultrasound Med Biol* 2009; 35: 1397–1404.
13. Tralaul CJ, MacRobert AJ, Coleridge-Smith PD, Barr H, Bown SG. Photodynamic therapy with phthalocyanine sensitization: quantitative studies in a transplantable rat fibrosarcoma. *Br J Cancer* 1987; 55: 389-395.
14. Zhang H, Chen B, Jiang H, Wang C, Wang H, Wang X. A strategy of ZnO nanorod mediated multi-mode cancer treatment. *Biomaterials* 2011; 32: 1906-1914.
15. Padmawathy, N, Vijayaraghavan, R. Enhanced bioactivity of ZnO nanoparticles—an antimicrobial study. *Sci. Technol. Adv. Mater.* 2008; 9: 035004 (7pp).
16. Gosh S, Goudar VS, Padmalekha KG, Bhat SV, Indi SS, Vasan HN. ZnO/Ag nanohydrate: synthesis, characterization, synergistic antibacterial activity and its mechanism. *RSC Adv* 2012; 2: 930-940.

17. Yin H, Casey PS, McCall MJ, Fenech M. Effects of surface chemistry on cytotoxicity, genotoxicity and the generation of reactive oxygen species induced by ZnO nanoparticles. *Langmuir* 2010; 19: 15399-15408.
18. Sangermano M, Malucelli G, Priola A, Lengvinaite S, Simokaitiene J, Grazulevicius JV. Carbazole derivatives as photosensitizers in cationic photopolymerization of clear and pigmented coatings. *Eur Polymer J* 2005; 41: 475-480.
19. Zhang FF, Gan LL, Zhou CH. Synthesis, Antibacterial and Antifungal Activities of some Carbazole Derivatives. *Bioorg Med Chem Lett* 2010; 6:1881-1884.
20. Zugle R, Nyokong T. Comparative Phototransformation of Environmental Pollutants Using Metallophthalocyanines Supported on Electrospun Polymer Fibers. *J Appl Polym Sci* 2012; 128: 1131-1140.
21. Khoza P, Antunes E, Chen J-Y, Nyokong T. Synthesis and Photophysical studies of a water soluble conjugate between folic acid and zinc tetraaminophthalocyanine. *J Lumin* 2013; 134: 784-790.
22. Masilela N, Nyokong T. Conjugates of low-symmetry Ge, Sn and Ti carboxyphthalocyanines with glutathione capped gold nanoparticles: An investigation of photophysical behaviour. *J Photochem Photobiol A* 2011; 223: 124-131.
23. Modisha P, Antunes E, Mack J, Nyokong T. Improvement of the photophysical parameters of zinc octacarboxy phthalocyanine upon conjugation to magnetic nanoparticles. *Int J Nanosci* 2013; 12: 1350010 (10 pages).
24. Shen T, Yuan ZI, Xu HJ. Fluorescent properties of phthalocyanines. *Dyes Pigm.* 1998; 11: 77- 80.

25. Patterson MS, Madsen SJ, Wilson R, Experimental tests of the feasibility of singlet oxygen luminescence monitoring *in vivo* during photodynamic therapy, J. Photochem. Photobiol. B: Biol. 1990; 5: 69-84.
26. Spiller W, Kliesch H, Worhle D, Hackbarth S, Röder B, Schnurpfeil G. Singlet oxygen quantum yield of different photosensitizers in polar solvents and micellar solutions. J. Porphyr Phthalocya 1998; 2: 145–158.
27. Ogunsipe A, Nyokong T. Photophysical and photochemical studies of sulphonated non-transition metal phthalocyanines in aqueous and non-aqueous media. J Photochem Photobiol A 2005; 173: 211 – 220.
28. Foote A, in Wasserman HH, Murray RW (Eds). Singlet Oxygen, Academic Press, New York, San Francisco, London, 1979: 139-171.
29. Bahnemann DW, Kormann C, Hoffmann MR. Preparation and characterization of quantum size zinc oxide: a detailed spectroscopic study. J Phys Chem 1987; 91: 3789-3798.
30. Shaheer AM, Alam KM, Seok JM, Bong YO. Controlled synthesis of various ZnO nanostructured materials by capping agent-assisted hydrothermal method for dye-sensitized solar cells. Electrochim Acta 2008; 53: 7869-787.
31. Huang Z-M, Zhang Y-Z, Kotaki M, Ramakrishna S. A review on polymer nanofibers by electrospinning and their applications in nanocomposites. Compos Sci Technol 2003; 63: 2223–2253.
32. Tang S, Shao C, Liu Y, Li S, Mu R. Electrospun nanofibers of poly(ethyleneoxide)/teraaminophthalocyanine copper(II) hybrids and its photoluminescence properties. J Phys Chem Solids 2007; 68: 2337-2340.

33. Achar BN, Lokesh KS. Studies on phthalocyanine sheet polymers. *J Organomet Chem* 2004; 689: 2601- 2605.
34. Ogunsipe A, Chen JY, Nyokong T. Photophysical and photochemical studies of zinc(II) phthalocyanine derivatives—effects of substituents and solvents. *New J Chem*, 2004; 28: 822-827.
35. Sun D, Sue HJ, Miyatake N. Optical Properties of ZnO Quantum Dots in Epoxy with Controlled Dispersion. *J Phys Chem C* 2008; 112: 16002-16010.
36. Vukonic S, Corni S, Mennucci B. Fluorescence Enhancement of Chromophores Close to Metal Nanoparticles. Optimal Setup Revealed by the Polarizable Continuum Model. *J Phys Chem C* 2009; 113: 121-133.

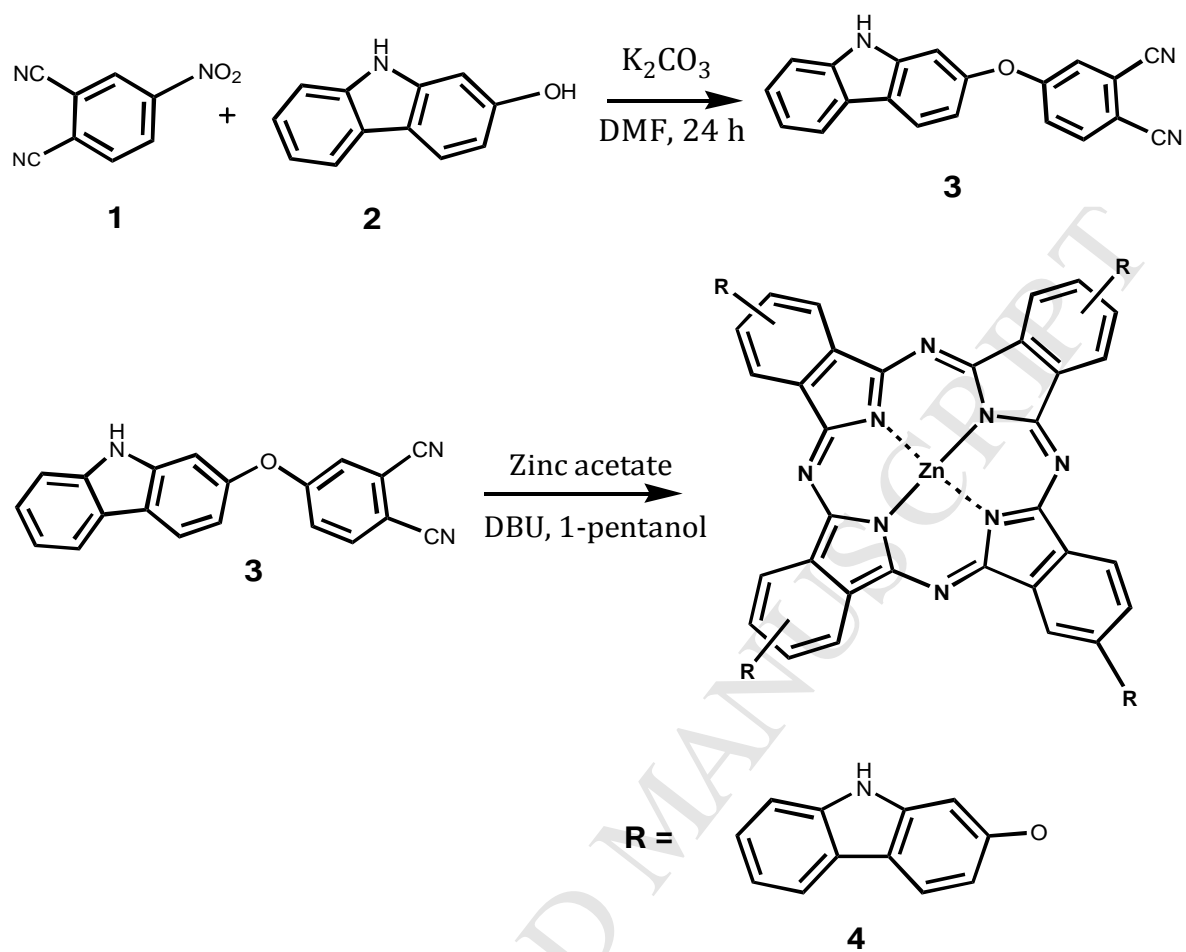
Table 1:

Solvent	Q <sub>abs</sub> (nm)	Q <sub>exc</sub> (nm)	Q <sub>emm</sub> (nm)	Stoke's shift (nm)
THF	677	678	687	9
DMF	680	679	693	14
DMSO	682	683	697	14
Pyridine	686	686	702	16

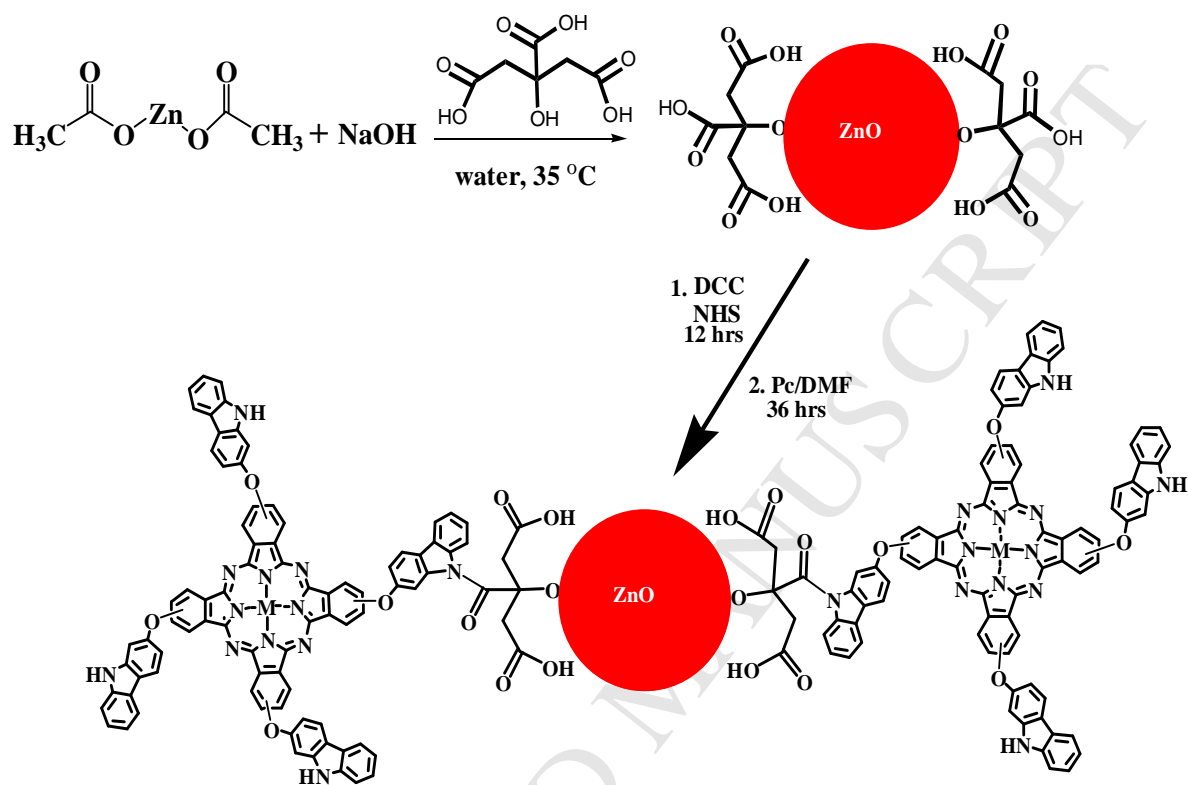
Table 2:

Conjugate/Complex	$\Phi_F$	$\tau_F$ (ns) <sup>a</sup>	$\Phi_{\Delta}$ <sup>b</sup>
Complex 4	<b>0.12</b>	<b>3.45 ± 0.03 (1.00)</b>	<b>0.83 (0.25)</b>
4-ZnOMPs	<b>0.12</b>	<b>2.82 ± 0.02 (0.80)</b>	<b>0.64 (0.20)</b>
		<b>0.48 ± 0.02 (0.20)</b>	
ZnPc	<b>0.30<sup>c</sup></b>	<b>3.8<sup>c</sup></b>	<b>0.56<sup>d</sup></b>

<sup>a</sup> Abundances in brackets. <sup>b</sup> numbers in brackets are for modifies fibers. <sup>c</sup> Ref 24. <sup>d</sup> Ref 26.



Scheme 1



Scheme 2

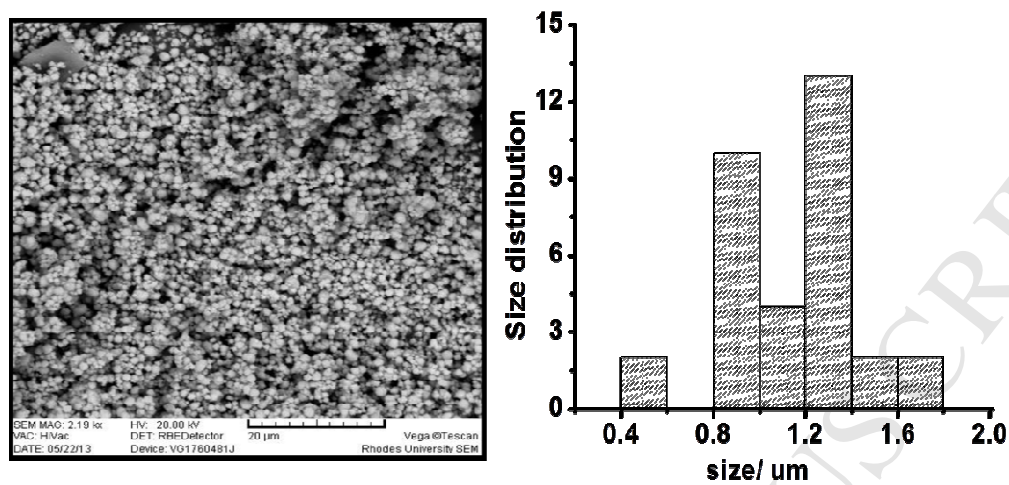


Figure 1:

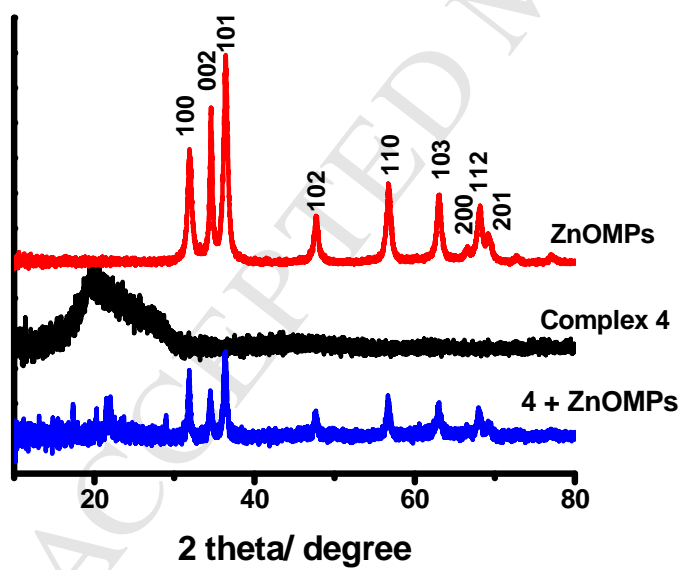


Figure 2:

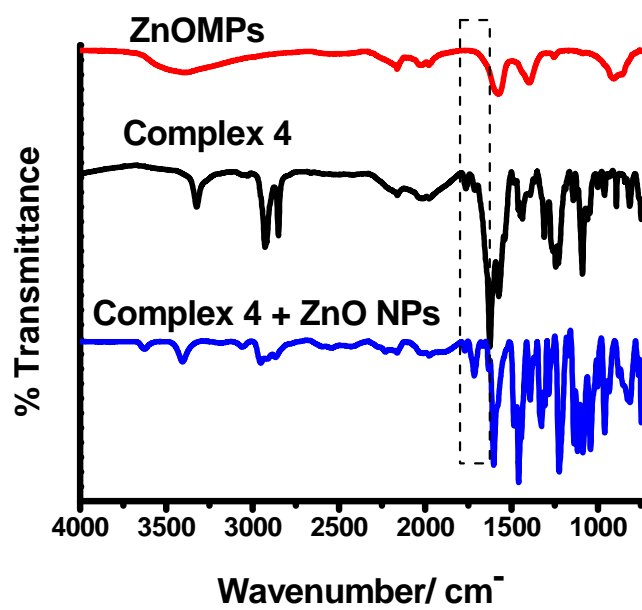


Figure 3:

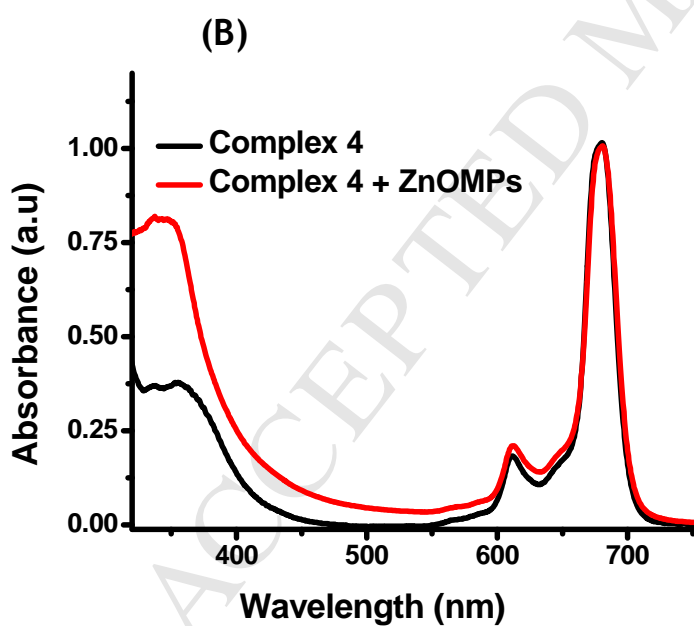
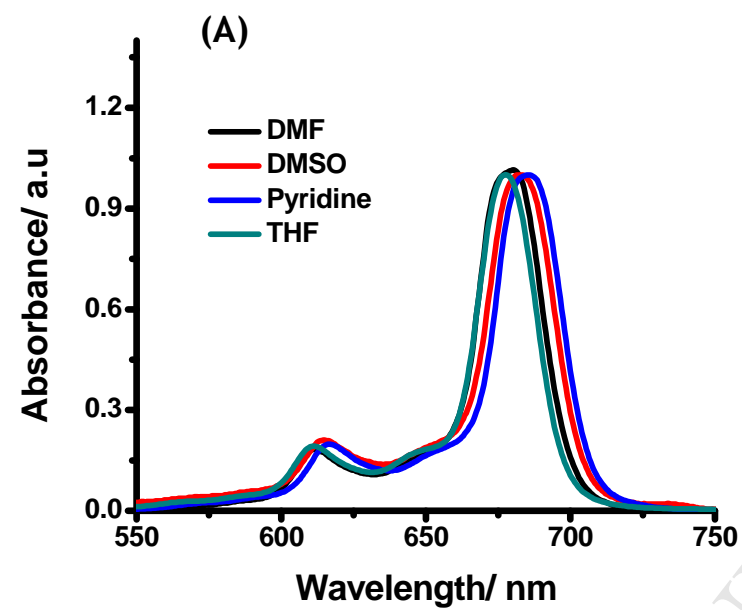


Figure 4:

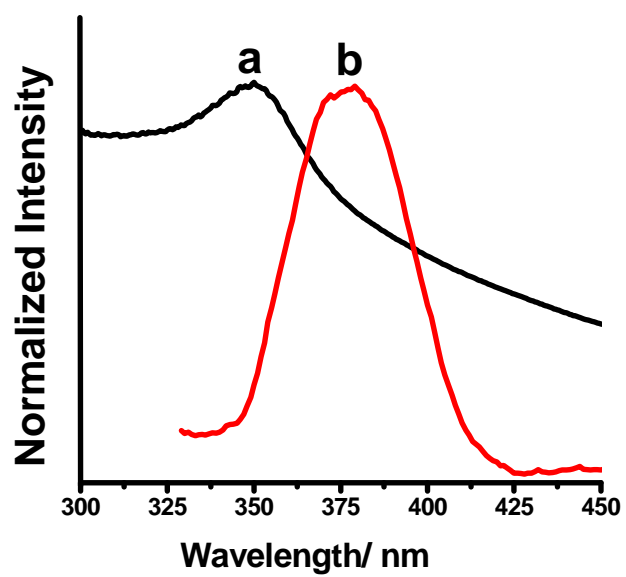


Figure 5:

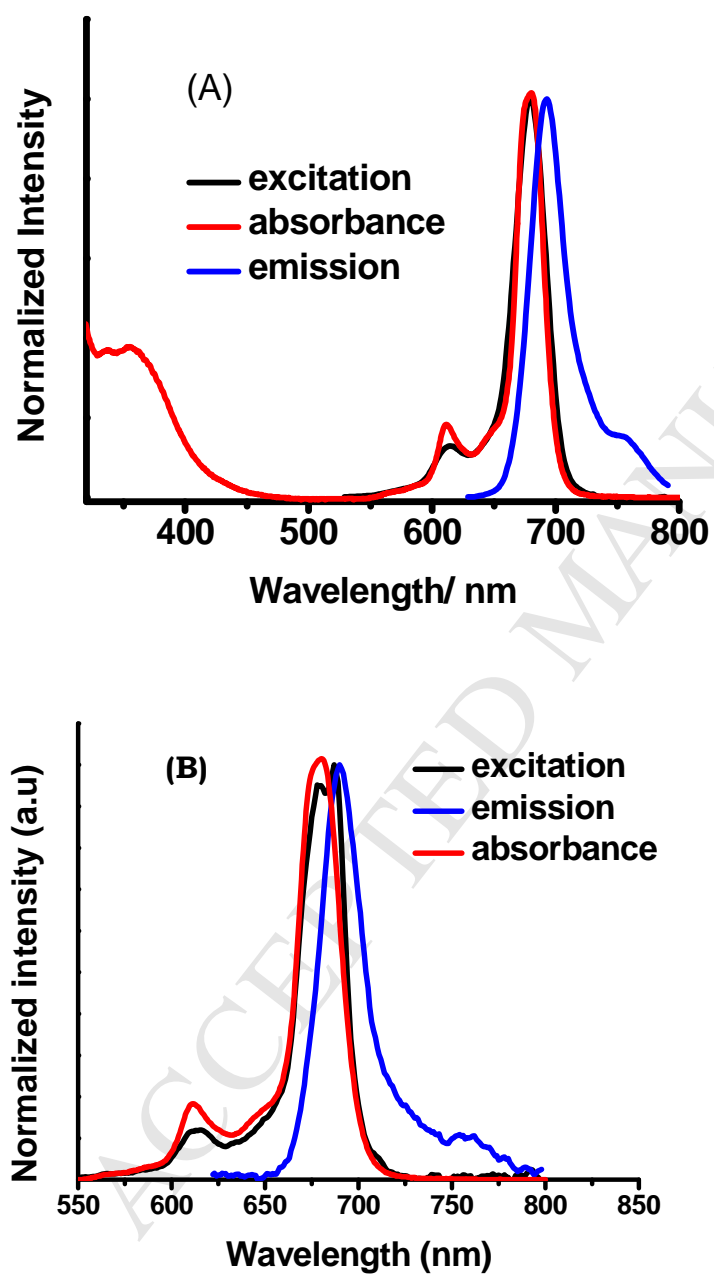


Figure 6:

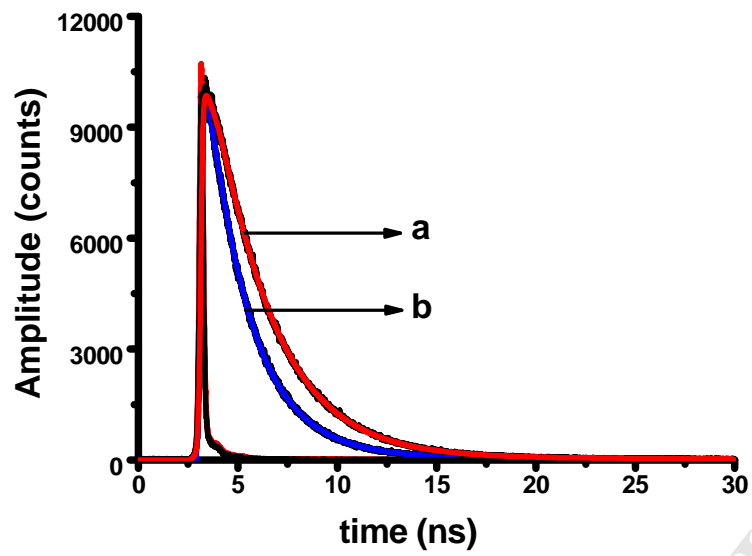


Figure 7:

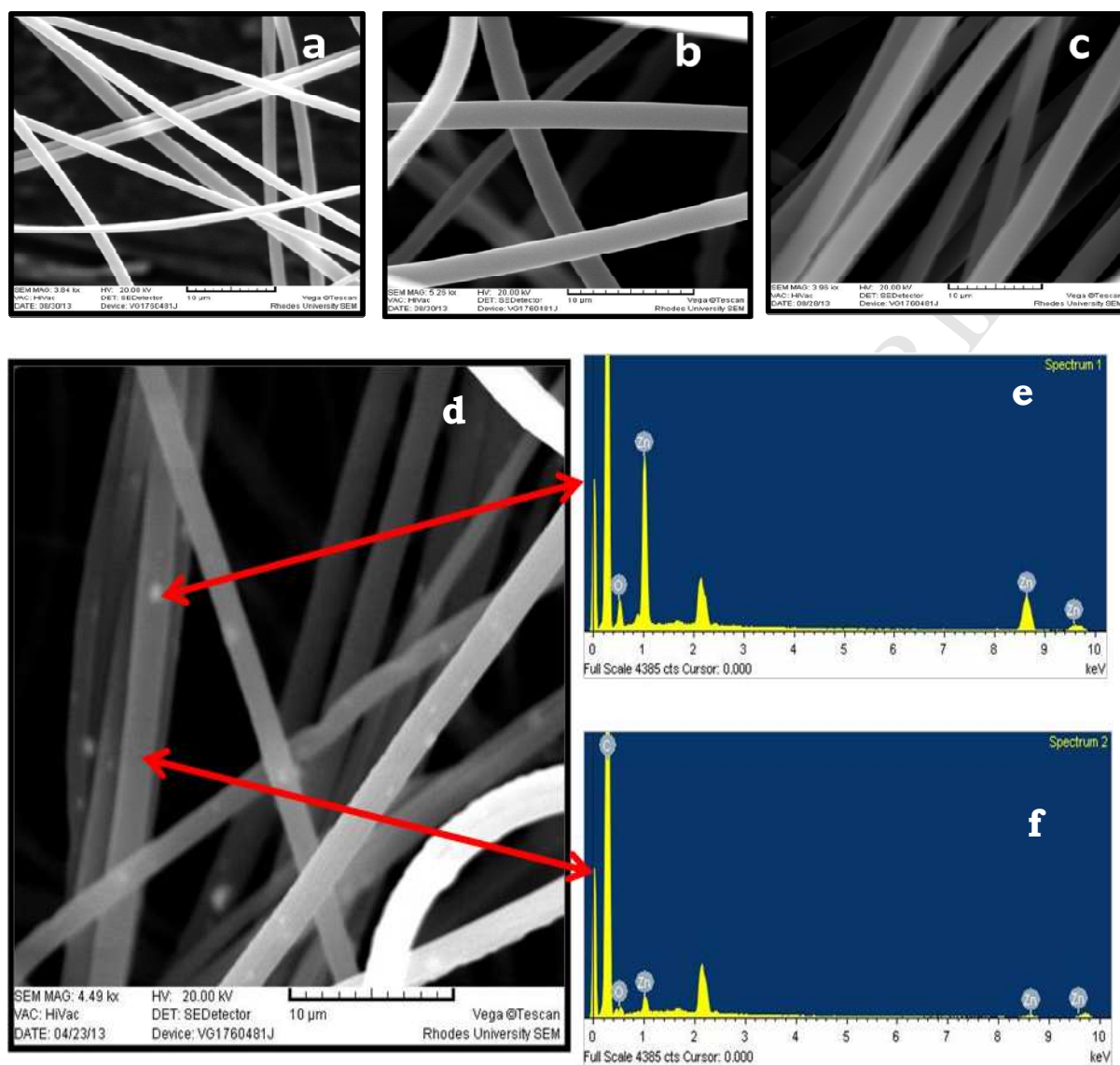
**Figure 8:**



Figure 9:

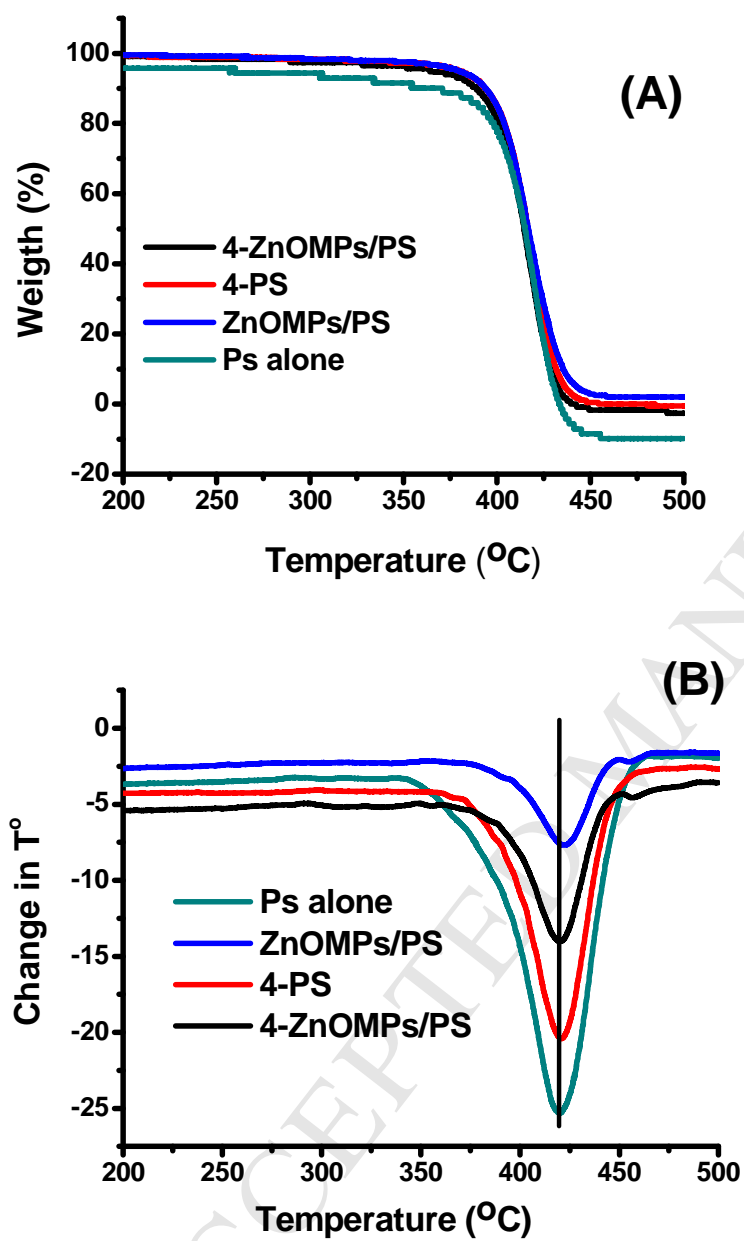


Figure 10:

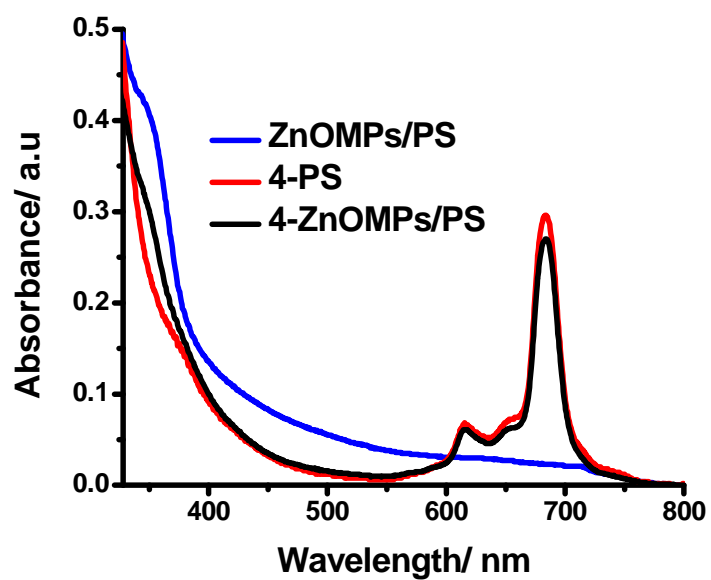


Figure 11:

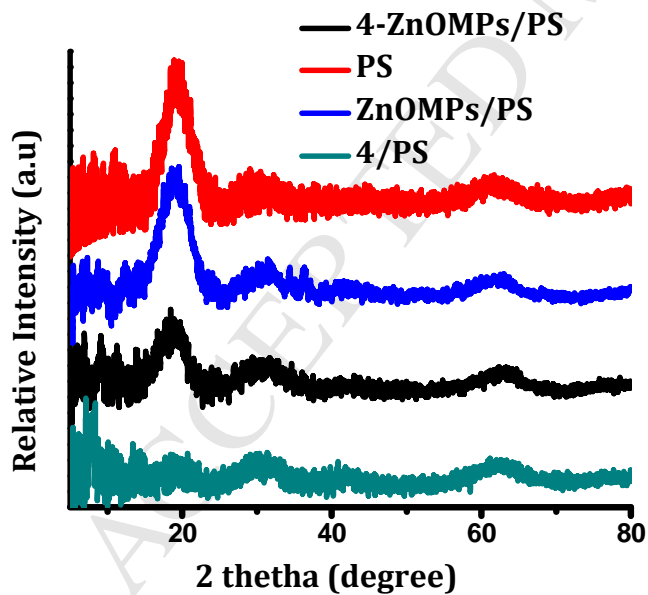


Figure 12:

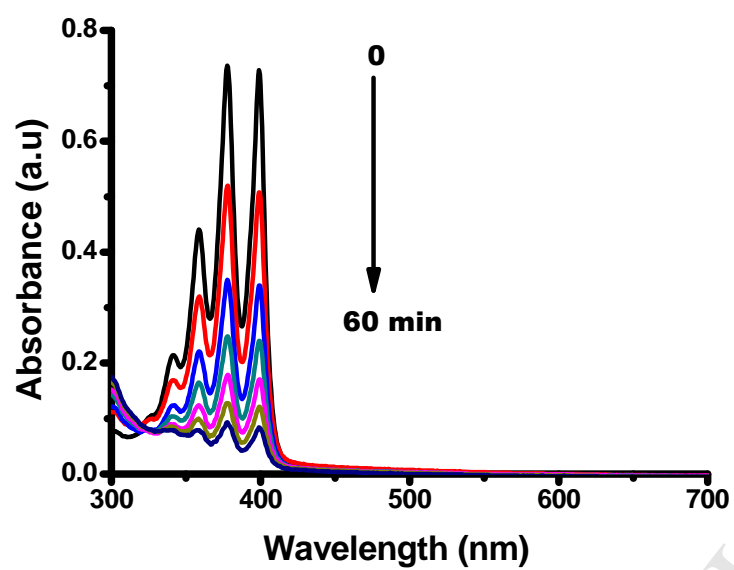


Figure 13:

**Tables , Schemes and Figures captions**

Table 1: Summary of absorption, excitation, emission and Stokes shift of complex 4

Table 2: Summary of photophysics and photochemical properties of complex 4 and 4-ZnOMPs in DMF.

Scheme 1: Schematic diagram showing synthesis of complex 4.

Scheme 2 : Synthesis of ZnO nanoparticles (ZnOMPs) and 4-ZnOMPs conjugate.

Figure 1: SEM micrograph of ZnOMPs (a) with the corresponding particles size distribution (b).

Figure 2: XRD pattern of ZnOMPs, complex 4 alone and 4-ZnOMPs conjugate.

Figure 3: IR spectra of citric acid capped ZnOMPs, 4 alone and 4-ZnOMPs conjugate.

Figure. 4: Absorption spectra of complex 4 (A) in different organic solvents and (B) in the presence and absence of ZnOMPs in DMF. Concentration  $\sim 8 \times 10^{-6}$  M.

Figure 5: Absorption (a) and emission (b) spectra of citrate capped ZnOMPs in DMF.

Figure 6: Absorption, excitation and emissions spectra of complex 4 in DMF (A) and 4-ZnOMPs conjugate in DMF (B).

Figure 7: Fluorescence decay curve of (a) complex 4 and (b) 4-ZnOMPs in DMF. Excitation wavelength, 680 nm,

Figure 8: SEM micrographs of PS (a), 4/PS (b), 4-ZnOMPs/PS (c) and ZnOMPs/PS (d). EDX plots corresponding to the 4-ZnOMPs/PS fiber with (e) and without (f) ZnOMPs.

Figure 9: Fluorescence micrographs of ZnOMPs/PS (a), 4/PS (b) and 4-ZnOMPs/PS(c).

Figure. 10: TGA (A) and DTA (B) thermograms of PS and PS functionalized nanofibers.

Figure 11: Absorption spectra of 4/PS, 4-ZnOMPs/PS and ZnOMPs/PS dissolved in toluene.

Figure 12: XRD pattern of PS, ZnOMPs/PS, **4**/PS and **4**-ZnOMPs/PS.

Figure 13: UV-Vis spectral changes observed upon photolysis of ADMA in water with **4**/PS over a period of 60 min. Time interval = 10 min.

## Research highlights

- A zinc phthalocyanine complex tetrasubstituted with a carbazole functionality at the peripheral position is reported
- The complex was subsequently conjugated to zinc oxide nanoparticles.
- The phthalocyanine and its conjugate with ZNO nanoparticles are electrospun into fibers
- The singlet oxygen quantum yield values in the fibers are near 0.2